PHYSICAL REVIEW B **88**, 224517 (2013)

Electronic structure and phase separation of superconducting and nonsuperconducting $K_xFe_{2-y}Se_2$ revealed by x-ray photoemission spectroscopy

M. Oiwake,[1] D. Ootsuki,[2] T. Noji,[3] T. Hatakeda,[3] Y. Koike,[3] M. Horio,[4] A. Fujimori,[4] N. L. Saini,[5] and T. Mizokawa[1,2]
[1]*Department of Complexity Science and Engineering, University of Tokyo, 5-1-5 Kashiwanoha, Chiba 277-8561, Japan*
[2]*Department of Physics, University of Tokyo, 5-1-5 Kashiwanoha, Chiba 277-8561, Japan*
[3]*Department of Applied Physics, Tohoku University, 6-6-05 Aoba, Aramaki, Aoba-ku, Sendai 980-8579, Japan*
[4]*Department of Physics, University of Tokyo, 7-3-1 Hongo, Tokyo 113-0033, Japan*
[5]*Dipartimento di Fisica, Universitá di Roma "La Sapienza" - P. le Aldo Moro 2, 00185 Roma, Italy*

(Received 30 October 2013; revised manuscript received 1 December 2013; published 31 December 2013)

We have investigated the electronic structure of superconducting (SC) and nonsuperconducting (non-SC) $K_xFe_{2-y}Se_2$ using x-ray photoemission spectroscopy (XPS). The spectral shape of the Fe $2p$ XPS is found to depend on the amount of Fe vacancies. The Fe $2p_{3/2}$ peak of the SC and non-SC Fe-rich samples is accompanied by a shoulder structure on the lower binding energy side, which can be attributed to the metallic phase embedded in the Fe^{2+} insulating phase. The absence of the shoulder structure in the non-SC Fe-poor sample allows us to analyze the Fe $2p$ spectra using a $FeSe_4$ cluster model. The Fe $3d$-Se $4p$ charge-transfer energy of the Fe^{2+} insulating phase is found to be $\sim$2.3 eV which is smaller than the Fe $3d$-Fe $3d$ Coulomb interaction of $\sim$3.5 eV. This indicates that the Fe^{2+} insulating state is the charge-transfer type in the Zaanen-Sawatzky-Allen scheme. We also find a substantial change in the valence-band XPS as a function of Fe content and temperature. The metallic state at the Fermi level is seen in the SC and non-SC Fe-rich samples and tends to be enhanced with cooling in the SC sample.

DOI: 10.1103/PhysRevB.88.224517 PACS number(s): 74.25.Jb, 74.70.Xa, 79.60.−i, 74.81.−g

I. INTRODUCTION

The electronic properties of Fe pnictides/chalcogenides have been attracting great interest since the discoveries of high-T_c superconductivity in Fe pnictides[1,2] and in Fe chalcogenides.[3,4] Among the variety of the Fe pnictides/chalcogenides superconductors, the $A_xFe_{2-y}Se_2$ ($A=$ K, Cs, Tl) system[5–9] exhibits the intrinsic phase separation into the magnetic insulating $A_xFe_{1.6}Se_2$ (245) phase and the superconducting $A_xFe_2Se_2$ (122) phase which has been revealed by various experimental techniques such as magnetization and resistivity measurement,[10] x-ray diffraction measurement,[11] scanning tunneling microscopy,[12] muon spin relaxation or rotation,[13,14] transmission electron microscopy,[15,16] nuclear magnetic resonance,[17] scanning electron microscopy,[18] optical spectroscopy and microscopy,[19,20] and x-ray absorption and emission spectroscopy.[21] In the magnetic insulating 245 phase, the Fe vacancies in the FeSe layer are ordered with the $\sqrt{5}\times\sqrt{5}$ Fe superstructure, and the Fe spins are antiferromagnetically ordered with the large magnetic moment of 3.3 μ_B per Fe.[22–24] The large magnetic moment suggests that the Fe $3d$ electrons are essentially localized in the insulating 245 phase.

On the other hand, angle-resolved photoemission spectroscopy (ARPES) of $A_xFe_{2-y}Se_2$ has revealed that the superconducting 122 phase has the Fermi surfaces whose geometry is very different from the other Fe pnictides/chalcogenides superconductors.[25–29] The absence of the hole pockets suggests that the superconducting 122 phase corresponds to the heavily electron doped FeSe (11 phase).[25–29] The valence-band structures of the superconducting and nonsuperconducting (antiferromagnetic insulating) samples of $K_xFe_{2-y}Se_2$, which were reported by Chen *et al.*, also show that the Fe $3d$ electrons are localized (itinerant) in the 245 (122) phase.[28] Very recently, by means of ARPES microscopy, Bendele *et al.* have observed the domain structures of the magnetic insulating 245 phase and the superconducting 122 phase and have identified the band structures of the magnetic insulating and superconducting domains.[30] The ARPES microscopy also has revealed the interesting spiderweb topology of the superconducting region.[30] The band dispersions of the magnetic insulating 245 phase and the superconducting 122 phase are systematically studied by the ARPES-based experiments. However, it still remains a mystery how the fundamental electronic structure of the two phases is related to the very unique phase separation in $K_xFe_{2-y}Se_2$. For example, the difference in the Fe valence between the two phases is not clearly identified by core-level spectroscopy. In this context, it is very important to study the difference of the Fe valence and the degree of Mottness between the magnetic insulating phase and the superconducting phase using core-level photoemission spectroscopy. In the present work we have studied the electronic structure and the Fe valence of the magnetic insulating 245 phase and the superconducting 122 phase in $K_xFe_{2-y}Se_2$ on the basis of x-ray photoemission spectroscopy (XPS) of superconducting (SC) and nonsuperconducting (non-SC) $K_xFe_{2-y}Se_2$. The XPS results on the non-SC Fe-poor sample enable us to analyze the electronic structure of the magnetic insulating state with Fe^{2+}. The contribution from the metallic phase is extracted from the XPS results on the SC and non-SC Fe-rich samples in order to discuss the electronic structure difference between the two phases.

II. METHOD

The single crystals of SC and non-SC $K_xFe_{2-y}Se_2$ were grown using the Bridgman method with $K:Fe:Se = 0.8:1.8:2.0$ and with $K:Fe:Se = 0.8:1.7:2.0$ or $0.8:1.6:2.0$, respectively. The actual compositions

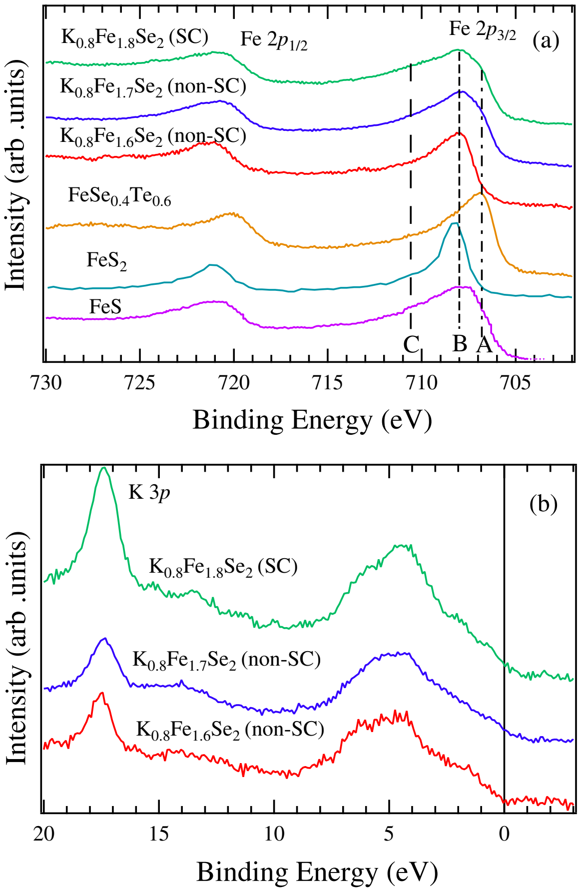

FIG. 1. (Color online) (a) The Fe $2p$ XPS spectra of the SC $K_{0.8}Fe_{1.8}Se_2$, non-SC $K_{0.8}Fe_{1.7}Se_2$, and non-SC $K_{0.8}Fe_{1.6}Se_2$. The Fe $2p$ XPS spectra of FeS_2 and FeS are taken from Refs. 31 and 32, respectively. (b) The valence-band XPS spectra of the SC $K_{0.8}Fe_{1.8}Se_2$, non-SC $K_{0.8}Fe_{1.7}Se_2$, and non-SC $K_{0.8}Fe_{1.6}Se_2$.

obtained by inductively coupled plasma analysis are $K:Fe:Se = 0.79(1):1.66(3):2$ for the SC Fe-rich crystals, and are $K:Fe:Se = 0.81(2):1.69(1):2$ and $K:Fe:Se = 0.79(2):1.59(3):2$ for the non-SC Fe-rich and Fe-poor crystals, respectively. The as-grown crystals were sealed in quartz tubes and were post-annealed for 1 h at 400 °C, followed by rapid cooling down to room temperature. The quartz tubes were opened and the single crystals were mounted on the sample holders under the Ar atmosphere. Then the samples were quickly transferred to the spectrometer under the ultrahigh vacuum in the 10^{-7} Pa range. We cleaved the single crystals at room temperature (300 K) under the ultrahigh vacuum for the XPS measurements. The XPS measurements were carried out using a JEOL JPS9200 analyzer. Mg $K\alpha$ (1253.6 eV) was used as the x-ray source. The total energy resolution was set to ∼1.0 eV. The binding energy was calibrated using the Au $4f$ core level of the gold reference sample.

III. RESULTS AND DISCUSSION

Figure 1(a) shows the Fe $2p$ core-level XPS spectra of the SC and non-SC Fe-rich samples ($K_{0.8}Fe_{1.8}Se_2$ and $K_{0.8}Fe_{1.7}Se_2$, respectively) and the non-SC Fe-poor sample ($K_{0.8}Fe_{1.6}Se_2$). The Fe $2p$ XPS spectrum of $K_xFe_{2-y}Se_2$ is compared to those of FeS_2,[31] FeS,[32] and $FeSe_{0.4}Te_{0.6}$.[33] From Fig. 1(a), it is found that the non-SC $K_{0.8}Fe_{1.6}Se_2$ has a narrow spectral width in the Fe $2p_{3/2}$ component, but the spectral width in the Fe $2p_{3/2}$ component of the SC $K_{0.8}Fe_{1.8}Se_2$ and the non-SC $K_{0.8}Fe_{1.7}Se_2$ is broad in comparison to that of the non-SC $K_{0.8}Fe_{1.6}Se_2$. The Fe $2p_{3/2}$ spectra of the SC $K_{0.8}Fe_{1.8}Se_2$ and the non-SC $K_{0.8}Fe_{1.7}Se_2$ can be resolved into two components which are labeled as A and B in Fig. 1(a). On the other hand, the Fe $2p_{3/2}$ spectrum of the non-SC $K_{0.8}Fe_{1.6}Se_2$ is basically a single peak which corresponds to peak B in the SC $K_{0.8}Fe_{1.8}Se_2$ and the non-SC $K_{0.8}Fe_{1.7}Se_2$. It should be noted here that the binding energy of the shoulder structure A is close to the Fe $2p_{3/2}$ binding energy of $FeSe_{0.4}Te_{0.6}$, which is also similar to that of Fe metal. On the other hand, the binding energy of peak B is close to the Fe $2p_{3/2}$ binding energies of FeS_2, which is insulating with the low-spin Fe^{2+} configuration, and of FeS, which is magnetic and is close to the high-spin Fe^{2+} configuration. Since the large magnetic moment of FeS indicates the high-spin Fe^{2+} configuration and its density of states (DOS) at the Fermi level (E_F) is relatively small,[32] FeS would be a good reference for the magnetic insulating state in $K_xFe_{2-y}Se_2$ although FeS is known as a magnetic metal.

In Fig. 1(b), the valence-band XPS spectra of the SC and non-SC Fe-rich samples ($K_{0.8}Fe_{1.8}Se_2$ and $K_{0.8}Fe_{1.7}Se_2$, respectively) and the non-SC Fe-poor sample ($K_{0.8}Fe_{1.6}Se_2$) are displayed. The significant DOS at E_F is observed in the SC $K_{0.8}Fe_{1.8}Se_2$ and the non-SC $K_{0.8}Fe_{1.7}Se_2$. This indicates the existence of a metallic phase. Meanwhile, in the non-SC $K_{0.8}Fe_{1.6}Se_2$, the DOS at E_F is almost negligible in comparison to those in the SC $K_{0.8}Fe_{1.8}Se_2$ and the non-SC $K_{0.8}Fe_{1.7}Se_2$. The shoulder structure A of the Fe $2p$ spectrum is observed in the SC $K_{0.8}Fe_{1.8}Se_2$ and the non-SC $K_{0.8}Fe_{1.7}Se_2$, which have the significant DOS at E_F, and is not seen in the non-SC $K_{0.8}Fe_{1.6}Se_2$, which has the negligibly small DOS at E_F. Therefore, one can safely conclude that the shoulder structure A in Fig. 1(a) corresponds to the Fe $2p_{3/2}$ spectrum of the metallic phase, and peak B in Fig. 1(a) is derived from the insulating phase with Fe^{2+}. It can be deduced that the non-SC $K_{0.8}Fe_{1.6}Se_2$ is dominated by the insulating 245 phase with Fe^{2+}, consistent with the fact that the formal Fe valance of the non-SC $K_{0.8}Fe_{1.6}Se_2$ is close to +2. On the other hand, the SC $K_{0.8}Fe_{1.8}Se_2$ and the non-SC $K_{0.8}Fe_{1.7}Se_2$ have inhomogeneous electronic states which are mixtures of the metallic phase and the insulating phase with Fe^{2+}. The energy splitting between structure A (from the metallic phase) and peak B (from the insulating phase) in the Fe $2p$ XPS spectra can be attributed to the extra screening effect by the conduction electron in the metallic phase. Therefore, it is difficult to estimate the actual Fe valence of the metallic phase.

In Figs. 2(a) and 2(b) the Fe $2p$ and valence-band XPS spectra of the SC sample shown in Fig. 1 are compared with those obtained from the aged SC sample which has been kept in a vacuum desiccator for more than 60 days and does not show superconductivity. Peak C at ∼711 eV in the aged sample is related to the oxidized phase with Fe^{3+} since the binding energy of peak C is ∼2 eV higher than peak B of the fresh SC sample, and the binding energy shift between B and C roughly corresponds to that between FeO (∼709.6 eV) and Fe_2O_3

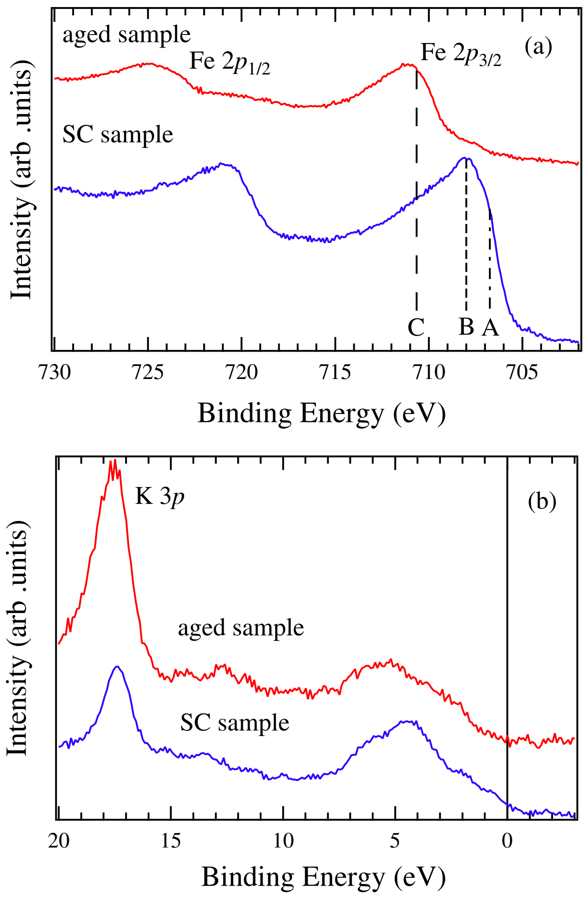

FIG. 2. (Color online) (a) The Fe $2p$ XPS spectra of the aged sample compared with that of the SC $K_{0.8}Fe_{1.8}Se_2$. (b) The valence-band XPS spectra of the aged sample compared with that of the SC $K_{0.8}Fe_{1.8}Se_2$.

(∼710.9 eV). Although the aged sample was cleaved under the ultrahigh vacuum in order to obtain the clean surface, the Fe $2p$ XPS spectrum is dominated by the Fe^{3+} component in the aged sample. In addition, the K $3p$ peak gains its intensity in the valence-band XPS spectra of the aged sample. These observations indicate that the increase of the Fe^{3+} component due to the oxidation is accompanied by the increase of the K $3p$ peak, which are consistent with the results in Figs. 1(a) and 1(b). Indeed, Fig. 1(a) shows that the Fe $2p$ XPS spectrum of the SC sample has a minor Fe^{3+} contribution (feature C). Also in Fig. 1(b), the K $3p$ peak is more intense in the SC sample than in the non-SC samples. Most probably, the minor Fe^{3+} component in the SC sample is derived from minor Fe^{3+} selenides with more Fe vacancies and/or less K content than the 245 phase, which might be partially oxidized before the aging. Since Fe^{3+} chalcogenides are easily oxidized by the air, the aging effect may start from the Fe^{3+} part with more Fe vacancies and/or less K content. Since the superconductivity is supported by the heavily electron-doped 122 phase with formal Fe valence of +1.5, the existence of the Fe^{3+} component may help to form the SC phase in $K_xFe_{2-y}Se_2$ where the average Fe valence is close to +2.

In order to estimate the ratio of the minority metallic phase to the majority insulating phase, we performed curve fitting for the Fe $2p_{3/2}$ spectra as shown in Fig. 3. The Fe $2p_{3/2}$ spectrum of the non-SC $K_{0.8}Fe_{1.6}Se_2$ is decomposed into a main peak with Mahan line shape $\frac{1}{\Gamma(\alpha)}\frac{e^{-(E_B-E_0)/\xi}}{|(E_B-E_0)/\xi|^{1-\alpha}}\Theta(E_B-E_0)$ convoluted by Voigt function, and a Gaussian for Fe^{3+} located at 711.0 eV with full width at half maximum of 3.3 eV

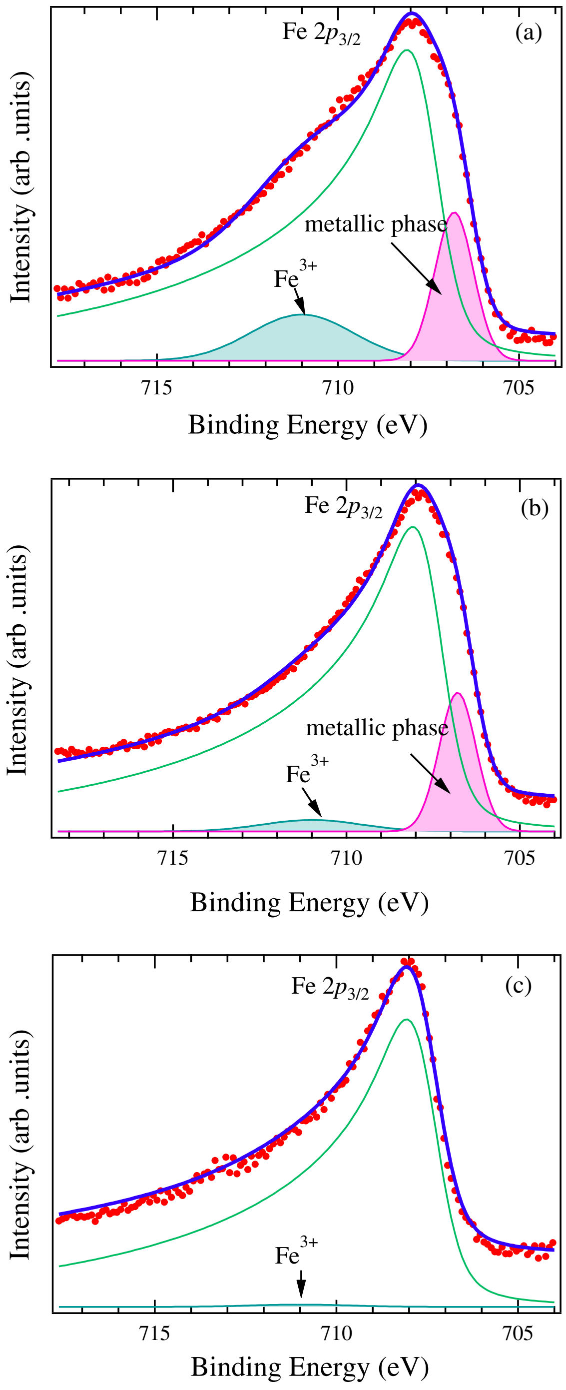

FIG. 3. (Color online) Curve fit for the Fe $2p_{3/2}$ XPS spectra of $K_xFe_{2-y}Se_2$. (a) Fe $2p_{3/2}$ XPS spectra of the SC $K_{0.8}Fe_{1.8}Se_2$. (b) Fe $2p_{3/2}$ XPS spectra of the non-SC $K_{0.8}Fe_{1.7}Se_2$. (c) Fe $2p_{3/2}$ XPS spectra of the non-SC $K_{0.8}Fe_{1.6}Se_2$. The dots represent the experimental results. The thick solid curve and the thin solid curves represent the fitted result and the Mahan and Gaussian components, respectively.

as functions of binding energy E_B. The main peak around 707.8 eV is derived from the Fe^{2+} state of the insulating 245 phase which shows the asymmetry due to the various screening channel including the Se $4p$ to Fe $3d$ charge transfer. The best fit results are obtained with $\alpha = 0.65$, $\xi = 8.1$ eV, and $E_0 = 707.5$ eV. The full widths at half maximum for Gaussian and Lorentzian of the Voigt function are 1.1 and 0.5 eV, respectively. The Gaussian for the Fe^{3+} component is negligibly small for the non-SC $K_{0.8}Fe_{1.6}Se_2$ as shown in Fig. 3(c). This result is very robust even if the position and width of the Fe^{3+} component are changed within a reasonable range. As shown in Figs. 3(b) and 3(a), the Fe $2p_{3/2}$ spectra of the non-SC $K_{0.8}Fe_{1.7}Se_2$ and the SC $K_{0.8}Fe_{1.8}Se_2$ can be fitted to the main peak with Mahan line shape convoluted by Voigt function (all the parameters are fixed to those for the non-SC $K_{0.8}Fe_{1.6}Se_2$), the Gaussian for the Fe^{3+} component, and the Gaussian peak at 706.8 eV. The peak at 706.8 eV can be attributed to the metallic and/or superconducting phase. The peak intensity of the metallic phase (peak at 706.8 eV) relative to the peak intensity of the insulating phase (represented by the Mahan line shape) is ~12.8% and ~12.0% for the SC $K_{0.8}Fe_{1.8}Se_2$ and the non-SC $K_{0.8}Fe_{1.7}Se_2$, respectively. In the present analysis, while the spectral weight of the Fe^{3+} component relative to the peak intensity of the insulating phase is as small as 2.6% in the non-SC $K_{0.8}Fe_{1.7}Se_2$, it reaches 10.5% in the SC $K_{0.8}Fe_{1.8}Se_2$.

Figures 4(a) and 4(b) show the temperature dependence of the Fe $2p_{3/2}$ spectra and the valence-band spectra in the SC $K_{0.8}Fe_{1.8}Se_2$, respectively. In going from 300 to 40 K, the intensity of shoulder structure A relative to that of peak B does not depend on temperature as shown in Fig. 4(a), whereas feature C loses its intensity with cooling. The decrease of the Fe^{3+} component with cooling is consistent with the observation in the x-ray absorption spectroscopy at the Fe K edge.[21] The negligibly small temperature dependence of shoulder structure A indicates that the volume fraction of the metallic phase does not depend on the temperature. On the other hand, the DOS at E_F increases with cooling as shown in Fig. 4(b) in the SC sample. This may be related to the temperature dependent resistivity anomaly in these materials. Here one can speculate that, while the volume fraction of the metallic regions is almost preserved with cooling, the network of the metallic regions develops to form the DOS at E_F at low temperature. Another possibility is that the disappearance of the Fe^{3+} component provides electrons to the metallic phases to enhance the DOS at E_F at low temperature. In addition, the intensity of the K $3p$ decreases with cooling as shown in Fig. 4(b). In Fig. 4(a), the spectral weight of the feature C (Fe^{3+}) also decreases with cooling. These observations indicate that the intensity of the K $3p$ peak correlates with the amount of the Fe^{3+} component, which is consistent with the results in Figs. 2(a) and 2(b). Here one possibility is that the formation of Fe^{3+} impurity (with more Fe vacancies or less K content) would be accompanied by segregation of K (namely, formation of a K-rich layer) between the FeSe layers. The cleavage at the K-rich layer is most probably favored and, therefore, the samples with more Fe^{3+} component tends to show higher K $3p$ intensity. As for the temperature dependence, such a K-rich surface would be suppressed with the decrease of the Fe^{3+} impurity phase. The suppression of the Fe^{3+} component (and the suppression of the K-rich layer) with cooling is really unusual, and it is very difficult to give a theoretical explanation at the present stage.

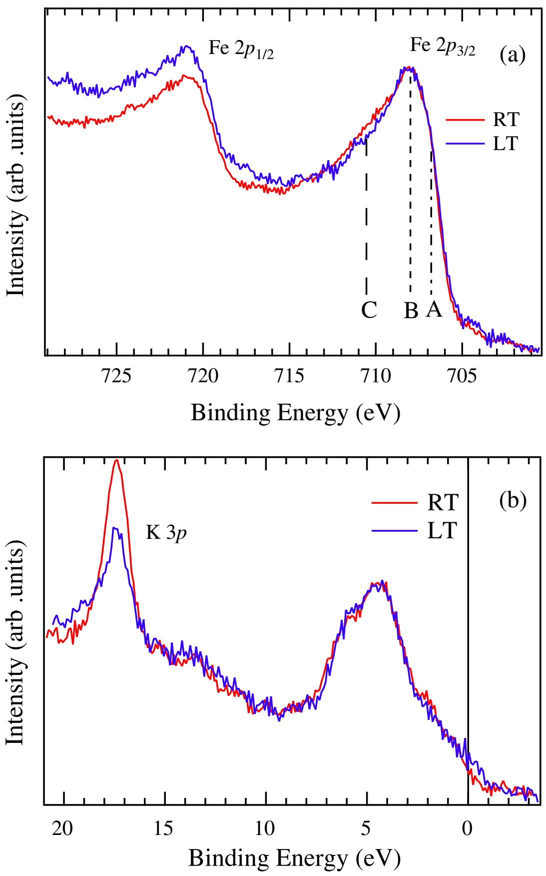

FIG. 4. (Color online) Temperature dependence of XPS spectra of the SC $K_{0.8}Fe_{1.8}Se_2$. RT and LT represent 300 and 40 K, respectively. (a) The Fe $2p$ XPS spectra. (b) The valence-band XPS spectra.

The shoulder structure of the Fe $2p$ spectrum is not observed in the non-SC $K_{0.8}Fe_{1.6}Se_2$. Therefore, the Fe $2p$ spectral shape of the non-SC $K_{0.8}Fe_{1.6}Se_2$ can be analyzed by the configuration-interaction calculation on a tetrahedral $FeSe_4$ cluster model.[31] The ground state is basically the high-spin d^6 state mixed with the d^7L, d^8L^2, d^9L^3, and $d^{10}L^4$ states where L represents a hole in the Se $4p$ ligand orbitals. The excitation energy from d^6 to d^7L corresponds to the charge-transfer energy Δ. With the Coulomb interaction U between the Fe $3d$ electrons, the excitation energy from d^7L to d^8L^2 is, for example, given by $\Delta + U$. The transfer integrals between the d^nL^m and $d^{n+1}L^{m+1}$ are described by $(pd\sigma)$ and $(pd\pi)$, where the ratio $(pd\sigma)/(pd\pi)$ is fixed at -2.16. The final states are given by the linear combinations of cd^6, cd^7L, cd^8L^2, cd^9L^3, and $cd^{10}L^4$, where c denotes a hole of the Fe $2p$ core level. The Coulomb interaction Q between the Fe $2p$ hole and the Fe $3d$ electron is expressed as Q which is fixed at $U/0.8$. The Fe $2p$ core-level spectrum can be calculated with the three adjustable parameters Δ, U, and $(pd\sigma)$. With $\Delta = 2.3$ eV, $U = 3.5$ eV, and $(pd\sigma) = -0.75$ eV, the calculated spectrum can reproduce the Fe $2p$ XPS result as shown in Fig. 5. The small Δ and U values of non-SC $K_{0.8}Fe_{1.6}Se_2$ are similar to those of FeS_2.[31]

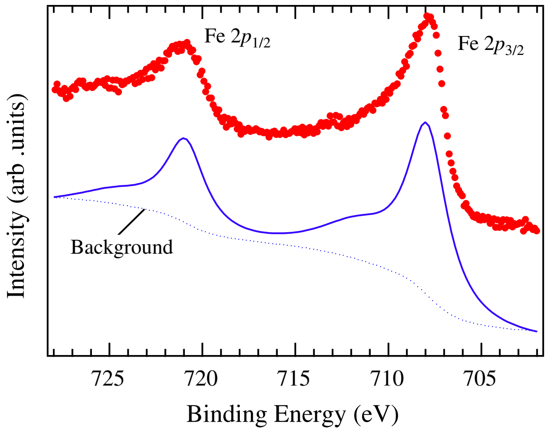

FIG. 5. (Color online) Experimental spectrum (dots) and calculated spectrum (solid curve) for the Fe $2p$ XPS for the non-SC $K_{0.8}Fe_{1.6}Se_2$. The dotted curve indicates the background due to the secondary electrons.

Δ is smaller than U, indicating that non-SC $K_{0.8}Fe_{1.6}Se_2$ falls in the charge-transfer regime of the Zaanen-Sawatzky-Allen scheme. The present analysis suggests that the Se $4p$ orbitals play important roles in the magnetic interaction between the Fe $3d$ spins.

IV. CONCLUSION

We have performed x-ray photoemission spectroscopy of superconducting and nonsuperconducting $K_xFe_{2-y}Se_2$ which show the interesting phase separation between the metallic phase and the magnetic insulating phase. We found that the Fe $2p$ XPS spectral shape strongly depends on the Fe content. The Fe $2p_{3/2}$ peak of the Fe-rich samples, which are superconducting and nonsuperconducting, is accompanied by a shoulder structure on the lower binding energy side. The shoulder structure can be assigned to the metallic phase embedded in the Fe^{2+} insulating phase, while the Fe $2p_{3/2}$ main peak is derived from the Fe^{2+} insulating phase. The shoulder structure is not observed in the nonsuperconducting Fe-poor sample. We have analyzed the Fe $2p$ spectra using a configuration-interaction calculation on a tetrahedral $FeSe_4$ cluster model, and found that the Fe^{2+} insulating phase is the charge-transfer-type Mott insulating state in the Zaanen-Sawatzky-Allen scheme.

The finite spectral weight at the Fermi level is observed in the Fe-rich sample, consistent with the interpretation of the Fe $2p$ XPS. While the volume fraction of the metallic regions does not depend on temperature, the spectral weight at the Fermi level develops with cooling. This indicates that the network between the metallic regions is formed at low temperature due to some electronic reconstruction in the charge-transfer-type Mott insulating state. In the future, the interplay between the magnetism and the possible local lattice distortion (including Jahn-Teller distortion) should be studied experimentally and theoretically in order to understand the relationship between the electronic structure and the phase separation.

ACKNOWLEDGMENTS

This work was partially supported by Grants-in-Aid (25400356) from the Japan Society of the Promotion of Science (JSPS). D.O. acknowledges support from the JSPS Research Fellowship for Young Scientists.

---

[1] Y. Kamihara, T. Watanabe, M. Hirano, and H. Hosono, J. Am. Chem. Soc. **130**, 3296 (2008).

[2] H. Takahashi, K. Igawa, K. Arii, Y. Kamihara, M. Hirano, and H. Hosono, Nature (London) **453**, 376 (2008).

[3] F. C. Hsu, J. Y. Luo, K.-W. Yeh, T.-K. Chen, T.-W. Huang, P.-M. Wu, Y.-C. Lee, Y.-L. Huang, Y.-Y. Chu, D.-C. Yan, and M.-K. Wu, Proc. Natl. Acad. Sci. USA **105**, 14262 (2008).

[4] S. Medvedev, T. M. McQueen, I. A. Troyan, T. Palasyuk, M. I. Eremets, R. J. Cava, S. Naghavi, F. Casper, V. Ksenofontov, G. Wortmann, and C. Felser, Nat. Mater. **8**, 630 (2009).

[5] J. Guo, S. Jin, G. Wang, S. Wang, K. Zhu, T. Zhou, M. He, and X. Chen, Phys. Rev. B **82**, 180520(R) (2010).

[6] A. Krzton-Maziopa, Z. Shermadini, E. Pomjakushina, V. Pomjakushin, M. Bendele, A. Amato, R. Khasanov, H. Luetkens, and K. Conder, J. Phys.: Condens. Matter **23**, 052203 (2011).

[7] C.-H. Li, B. Shen, F. Han, X. Zhu, and H.-H. Wen, Phys. Rev. B **83**, 184521 (2011).

[8] Y. Mizuguchi, H. Takeya, Y. Kawasaki, T. Ozaki, S. Tsuda, T. Yamaguchi, and Y. Takano, Appl. Phys. Lett. **98**, 042511 (2011).

[9] R. H. Liu, X. G. Luo, M. Zhang, A. F. Wang, J. J. Ying, X. F. Wang, Y. J. Yan, Z. J. Xiang, P. Cheng, G. J. Ye, Z. Y. Li, and X. H. Chen, Europhys. Lett. **94**, 27008 (2011).

[10] B. Shen, B. Zeng, G. F. Chen, J. B. He, D. M. Wang, H. Yang, and H. H. Wen, Europhys. Lett. **96**, 37010 (2011).

[11] A. Ricci, N. Poccia, B. Joseph, G. Arrighetti, L. Barba, J. Plaisier, G. Campi, Y. Mizuguchi, H. Takeya, Y. Takano, N. L. Saini, and A. Bianconi, Supercond. Sci. Technol. **24**, 082002 (2011).

[12] W. Li, H. Ding, P. Deng, K. Chang, C. Song, K. He, L. Wang, X. Ma, J.-P. Hu, X. Chen, and Q. K. Xue, Nat. Phys. **8**, 126 (2011).

[13] Z. Shermadini, A. Krzton-Maziopa, M. Bendele, R. Khasanov, H. Luetkens, K. Conder, E. Pomjakushina, S. Weyeneth, V. Pomjakushin, O. Bossen, and A. Amato, Phys. Rev. Lett. **106**, 117602 (2011).

[14] Z. Shermadini, H. Luetkens, R. Khasanov, A. Krzton-Maziopa, K. Conder, E. Pomjakushina, H.-H. Klauss, and A. Amato, Phys. Rev. B **85**, 100501(R) (2012).

[15] Z. Wang, Y. J. Song, H. L. Shi, Z. W. Wang, Z. Chen, H. F. Tian, G. F. Chen, J. G. Guo, H. X. Yang, and J. Q. Li, Phys. Rev. B **83**, 140505(R) (2011).

[16] Z.-W. Wang, Z. Wang, Y.-J. Song, C. Ma, Y. Cai, Z. Chen, H.-F. Tian, H.-X. Yang, G.-F. Chen, and J.-Q. Li, J. Phys. Chem. C **116**, 17847 (2012).

[17] Y. Texier, J. Deisenhofer, V. Tsurkan, A. Loidl, D. S. Inosov, G. Friemel, and J. Bobroff, Phys. Rev. Lett. **108**, 237002 (2012).

[18] Y. Liu, Q. Xing, K. W. Dennis, R. W. McCallum, and T. A. Lograsso, Phys. Rev. B **86**, 144507 (2012).

[19] R. H. Yuan, T. Dong, Y. J. Song, P. Zheng, G. F. Chen, J. P. Hu, J. Q. Li, and N. L. Wang, Sci. Rep. **2**, 221 (2012).

[20] A. Charnukha, A. Cvitkovic, T. Prokscha, D. Pröpper, N. Ocelic, A. Suter, Z. Salman, E. Morenzoni, J. Deisenhofer, V. Tsurkan, A. Loidl, B. Keimer, and A. V. Boris, Phys. Rev. Lett. **109**, 017003 (2012).

[21] L. Simonelli, N. L. Saini, M. M. Sala, Y. Mizuguchi, Y. Takano, H. Takeya, T. Mizokawa, and G. Monaco, Phys. Rev. B **85**, 224510 (2012).

[22] M.-H. Fang, H.-D. Wang, C.-H. Dong, Z.-J. Li, C.-M. Feng, J. Chen, and H. Q. Yuan, Europhys. Lett. **94**, 27009 (2011).

[23] W. Bao, Q. Huang, G. F. Chen, M. A. Green, D. M. Wang, J. B. He, X. Q. Wang, and Y. Qiu, Chin. Phys. Lett. **28**, 086104 (2011).

[24] J. Zhao, H. Cao, E. Bourret-Courchesne, D.-H. Lee, and R. J. Birgeneau, Phys. Rev. Lett. **109**, 267003 (2012).

[25] Y. Zhang, L. X. Yang, M. Xu, Z. R. Ye, F. Chen, C. He, H. C. Xu, J. Jiang, B. P. Xie, J. J. Ying, X. F. Wang, X. H. Chen, J. P. Hu, M. Matsunami, S. Kimura, and D. L. Feng, Nat. Mater. **10**, 273 (2011).

[26] T. Qian, X.-P. Wang, W.-C. Jin, P. Zhang, P. Richard, G. Xu, X. Dai, Z. Fang, J.-G. Guo, X.-L. Chen, and H. Ding, Phys. Rev. Lett. **106**, 187001 (2011).

[27] D. Mou, S. Liu, X. Jia, J. He, Y. Peng, L. Zhao, L. Yu, G. Liu, S. He, X. Dong, J. Zhang, H. Wang, C. Dong, M. Fang, X. Wang, Q. Peng, Z. Wang, S. Zhang, F. Yang, Z. Xu, C. Chen, and X. J. Zhou, Phys. Rev. Lett. **106**, 107001 (2011).

[28] F. Chen, M. Xu, Q. Q. Ge, Y. Zhang, Z. R. Ye, L. X. Yang, Juan Jiang, B. P. Xie, R. C. Che, M. Zhang, A. F. Wang, X. H. Chen, D. W. Shen, J. P. Hu, and D. L. Feng, Phys. Rev. X **1**, 021020 (2011).

[29] Z.-H. Liu, P. Richard, N. Xu, G. Xu, Y. Li, X.-C. Fang, L.-L. Jia, G.-F. Chen, D.-M. Wang, J.-B. He, T. Qian, J.-P. Hu, H. Ding, and S.-C. Wang, Phys. Rev. Lett. **109**, 037003 (2012).

[30] M. Bendele, A. Barinov, B. Joseph, D. Innocenti, A. Iadecola, H. Takeya, Y. Mizuguchi, T. Takano, T. Noji, T. Hatakeda, Y. Koike, M. Horio, A. Fujimori, D. Ootsuki, T. Mizokawa, and N. L. Saini (unpublished).

[31] A. E. Bocquet, T. Mizokawa, T. Saitoh, H. Namatame, and A. Fujimori, Phys. Rev. B **46**, 3771 (1992).

[32] K. Shimada, T. Mizokawa, K. Mamiya, T. Saitoh, A. Fujimori, K. Ono, A. Kakizaki, T. Ishii, M. Shirai, and T. Kamimura, Phys. Rev. B **57**, 8845 (1998).

[33] M. Oiwake, D. Ootsuki, T. Mizokawa, T. Noji, M. Imaizumi, and M. Koike (unpublished).